# Supplementary Material

## Enhanced Electromagnetic Absorption Properties of the Double-Layer $Ti_3C_2T_x$ MXene Absorber with Orthogonal Microstructures

*Yuanhao Ning*[1, 2], *Shuang Yang*[1, 2], *Xianxian Sun*[3], *Shasha Wang*[1, 2], *Lei Liang*[1, 2], *Yuanjing Cheng*[1, 2], *Ye Yuan*[3]* *and Yibin Li*[1, 2, 3]*.

[1] National Key Laboratory of Science and Technology on Advanced Composites in Special Environments, Harbin Institute of Technology, Harbin 150080, P. R. China

[2] Center for Composite Materials and Structures, Harbin Institute of Technology, Harbin 150080, P. R. China

[3] School of Materials Science and Engineering, Beihang University, Beijing 100081, P. R. China

***Corresponding author, e-mail:**

yuanyewins@hebut.edu.cn (Ye Yuan)

liyibin@hit.edu.cn (Yibin Li).

## Supplementary Material:

**Fig. S1.** Digital photo for $Ti_3C_2T_x$ MXene foam.

**Fig. S2.** EDS of the $Ti_3C_2T_x$ MXene foam.

**Fig. S3.** XRD pattern of $Ti_3AlC_2$, $Ti_3C_2T_x$, and the $Ti_3C_2T_x$ MXene foam.

**Fig. S4.** 1/4 wavelength matching model for (a) the perpendicular and (b) the parallel sample.

**Fig. S5.** Cole-Cole images of (a) the perpendicular and (b) the parallel sample.

**Fig. S6.** $\varepsilon'' / f - \varepsilon'$ curves of (a) the perpendicular and (b) the parallel sample.

**Fig. S7.** $\varepsilon'' - f^{-1}$ curves of (a) the perpendicular and (b) the parallel sample.

**Fig. S8** Electromagnetic wave reflection loss for the sample with the parallel end thickness of (a) 5%, (b) 10%, (c) 35%, (d) 40%, (e) 45%, (f) 50%, (g) 55%, (h) 60%, (i) 65%, (j) 70%, (k) 75%, (l) 80%, (m) 85%, (n) 90%, and (o) 95%, with electromagnetic wave incident from the parallel ends, separately.

**Table S1** Electromagnetic wave reflection loss for samples with electromagnetic waves incident from the parallel ends.

**Fig. S9** Electromagnetic wave reflection loss for the sample with the perpendicular end thickness of (a) 5%, (b) 10%, (c) 15%, (d) 20%, (e) 25%, (f) 30%, (g) 35%, (h) 40%, (i) 45%, (j) 50%, (k) 55%, (l) 60%, (m) 65%, (n) 70%, (o) 75%, (p) 80%, (q) 85%, (r) 90%, and (s) 95%, with electromagnetic wave incident from the perpendicular ends, separately.

**Table S2** Electromagnetic wave reflection loss for samples with electromagnetic waves incident from the perpendicular ends.

**Fig. S10** (a, c) Comparison of RL curves for single and double layer samples with the same thickness; (b, d) Comparison of RL curves for double-layer samples and their compositions, where parallel end thickness of 25% in (a, b) and 20% in (c, d).

**Table S3** Electromagnetic wave absorption properties of some earlier $Ti_3C_2T_x$ MXene materials

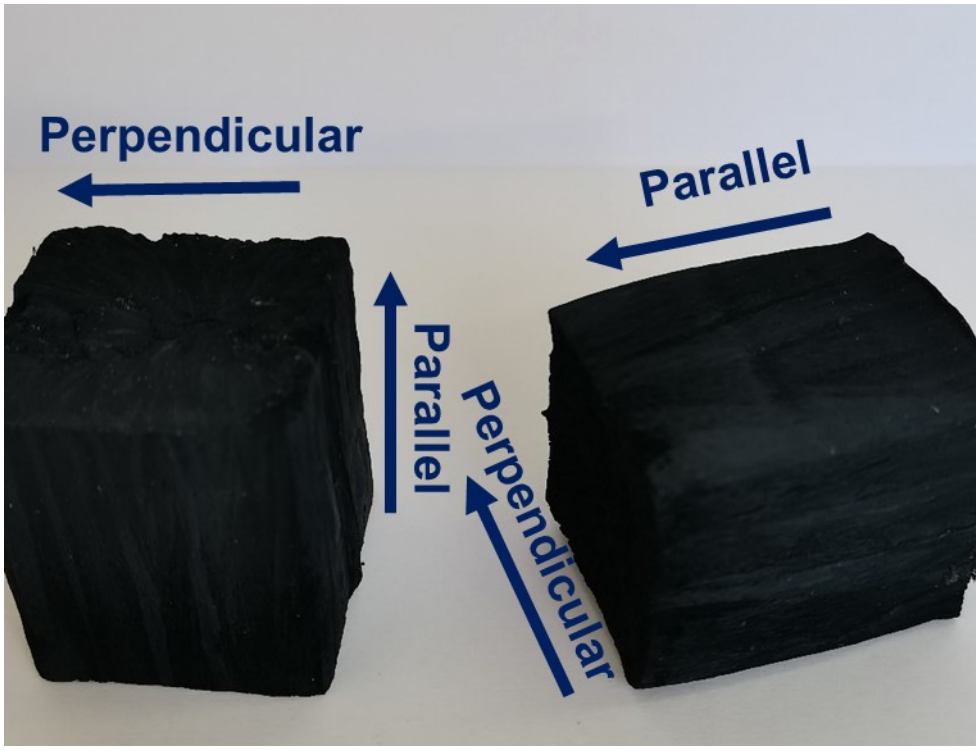


**Fig. S1** Digital photo of the $Ti_3C_2T_x$ MXene foam.

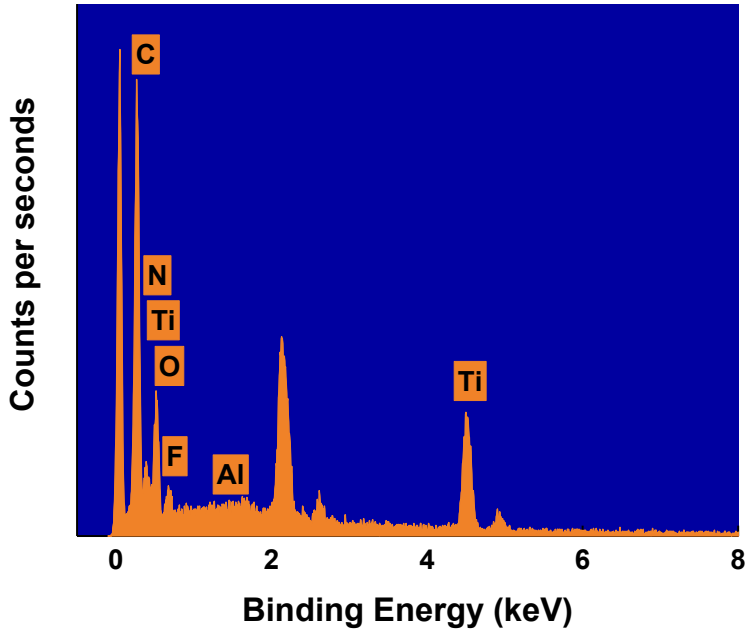


**Fig. S2** EDS of the $Ti_3C_2T_x$ MXene foam.

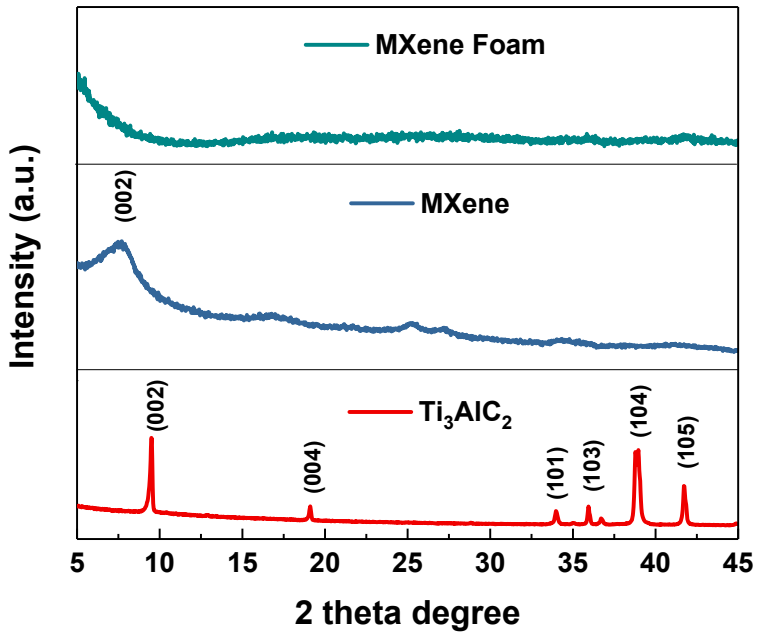


**Fig. S3** XRD pattern of $Ti_3AlC_2$, $Ti_3C_2T_x$, and the $Ti_3C_2T_x$ MXene foam.

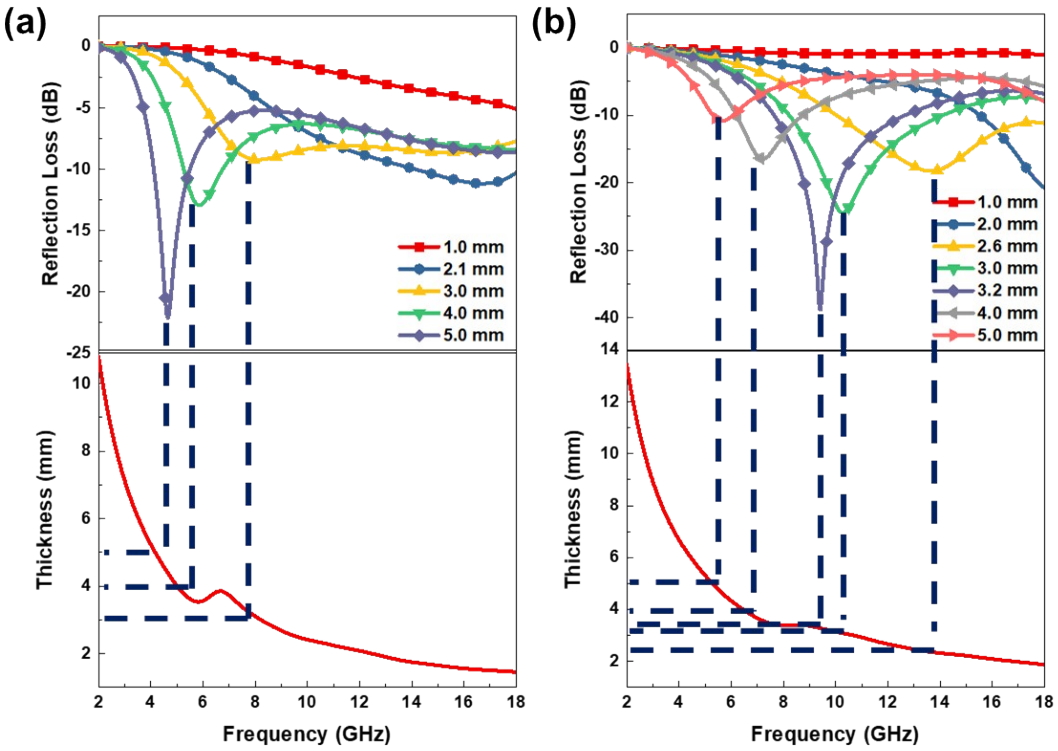


**Fig. S4** 1/4 wavelength matching model for (a) the perpendicular and (b) the parallel sample.

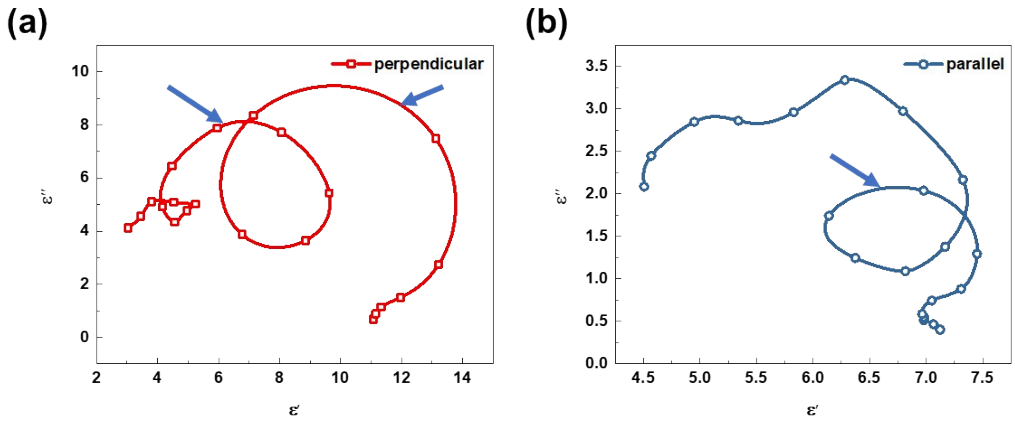


**Fig. S5** Cole-Cole images of (a) the perpendicular and (b) the parallel sample.

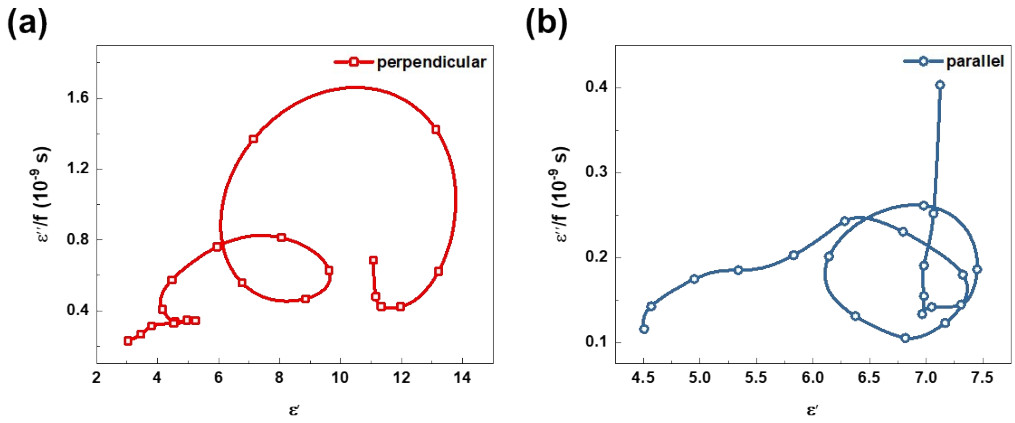


**Fig. S6** $\varepsilon'' / f - \varepsilon'$ curves of (a) the perpendicular and (b) the parallel sample.

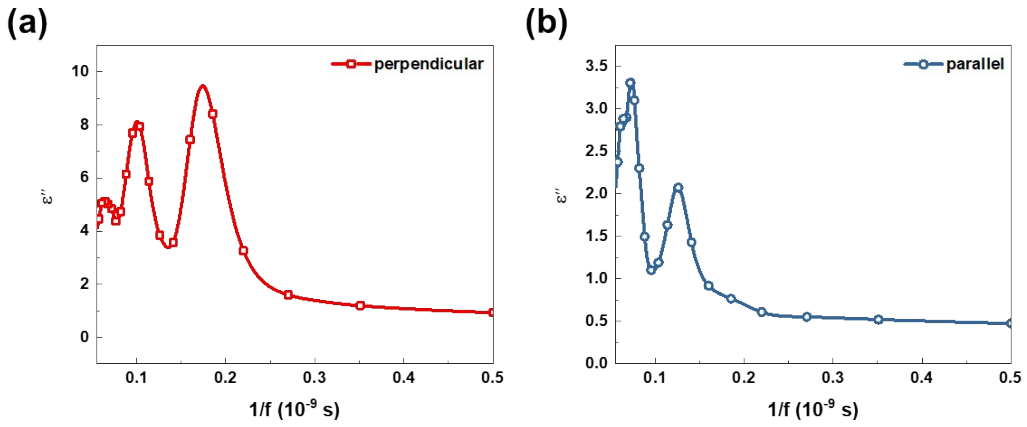


**Fig. S7** $\varepsilon'' - f^{-1}$ curves of (a) the perpendicular and (b) the parallel sample.

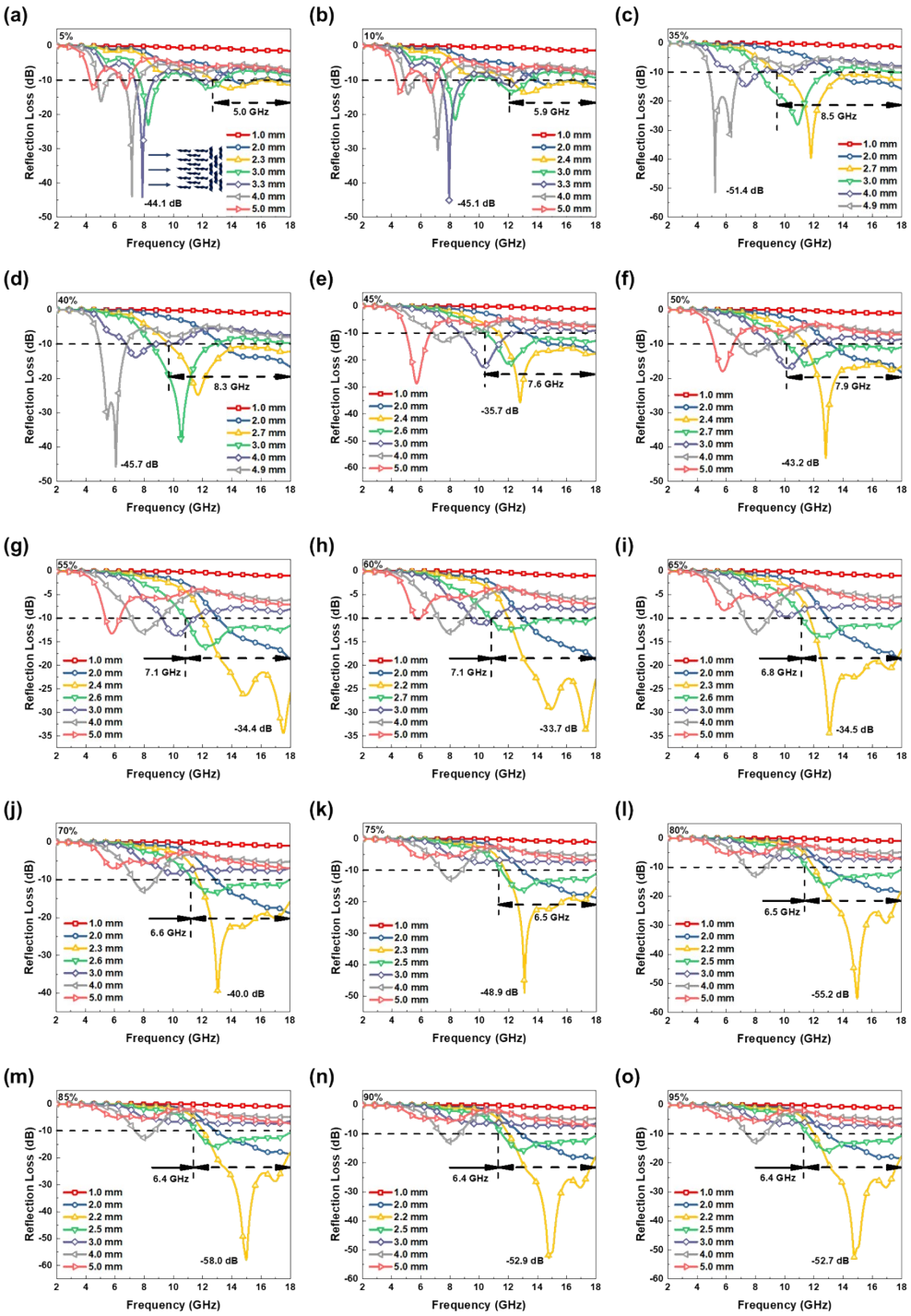


**Fig. S8** Electromagnetic wave reflection loss for the sample with the parallel end thickness of (a) 5%, (b) 10%, (c) 35%, (d) 40%, (e) 45%, (f) 50%, (g) 55%, (h) 60%, (i) 65%, (j) 70%, (k) 75%, (l) 80%, (m) 85%, (n) 90%, and (o) 95%, with electromagnetic wave incident from the parallel ends, separately.

**Table S1** Electromagnetic wave reflection loss for samples with electromagnetic waves incident from the parallel ends.

| Matching layer thickness ratio | $RL_{min}$ (dB) | Related Frequency of $RL_{min}$ (GHz) | Related Thickness of $RL_{min}$ (mm) | $EAB_{max}$ (GHz) | Related Thickness of $EAB_{max}$ (mm) |
|---|---|---|---|---|---|
| 5% | -44.1 | 7.9 | 3.3 | 5.0 | 2.3 |
| 10% | -45.1 | 7.9 | 3.3 | 5.9 | 2.4 |
| 15% | -47.2 | 8.0 | 3.3 | 7.0 | 2.6 |
| 20% | -50.6 | 8.1 | 3.3 | 9.4 | 2.6 |
| 25% | -60.8 | 6.6 | 4.6 | 9.1 | 2.7 |
| 30% | -43.4 | 6.5 | 4.7 | 8.8 | 2.7 |
| 35% | -51.4 | 5.2 | 4.9 | 8.5 | 2.7 |
| 40% | -45.7 | 6.1 | 4.9 | 8.3 | 2.7 |
| 45% | -35.7 | 12.8 | 2.4 | 7.6 | 2.6 |
| 50% | -43.2 | 12.8 | 2.4 | 7.9 | 2.7 |
| 55% | -34.4 | 17.5 | 2.4 | 7.1 | 2.6 |
| 60% | -33.7 | 17.3 | 2.2 | 7.1 | 2.7 |
| 65% | -34.5 | 13.1 | 2.3 | 6.8 | 2.6 |
| 70% | -40.0 | 13.1 | 2.3 | 6.6 | 2.6 |
| 75% | -48.9 | 13.1 | 2.3 | 6.5 | 2.5 |
| 80% | -55.2 | 15.0 | 2.2 | 6.5 | 2.5 |
| 85% | -58.0 | 15.0 | 2.2 | 6.4 | 2.5 |
| 90% | -52.9 | 14.8 | 2.2 | 6.4 | 2.5 |
| 95% | -52.7 | 14.8 | 2.2 | 6.4 | 2.5 |

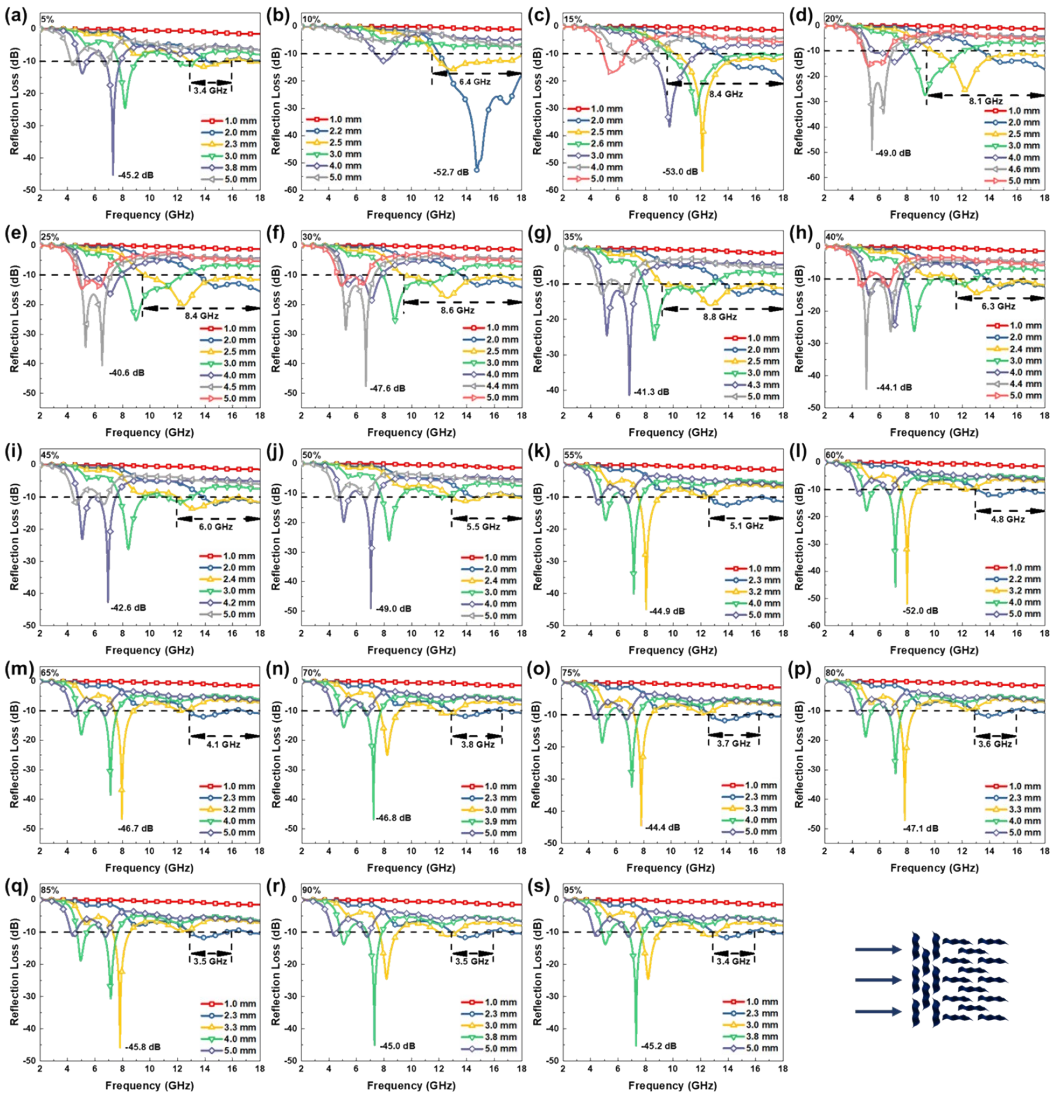


**Fig. S9** Electromagnetic wave reflection loss for the sample with the perpendicular end thickness of (a) 5%, (b) 10%, (c) 15%, (d) 20%, (e) 25%, (f) 30%, (g) 35%, (h) 40%, (i) 45%, (j) 50%, (k) 55%, (l) 60%, (m) 65%, (n) 70%, (o) 75%, (p) 80%, (q) 85%, (r) 90%, and (s) 95%, with electromagnetic wave incident from the perpendicular ends, separately.

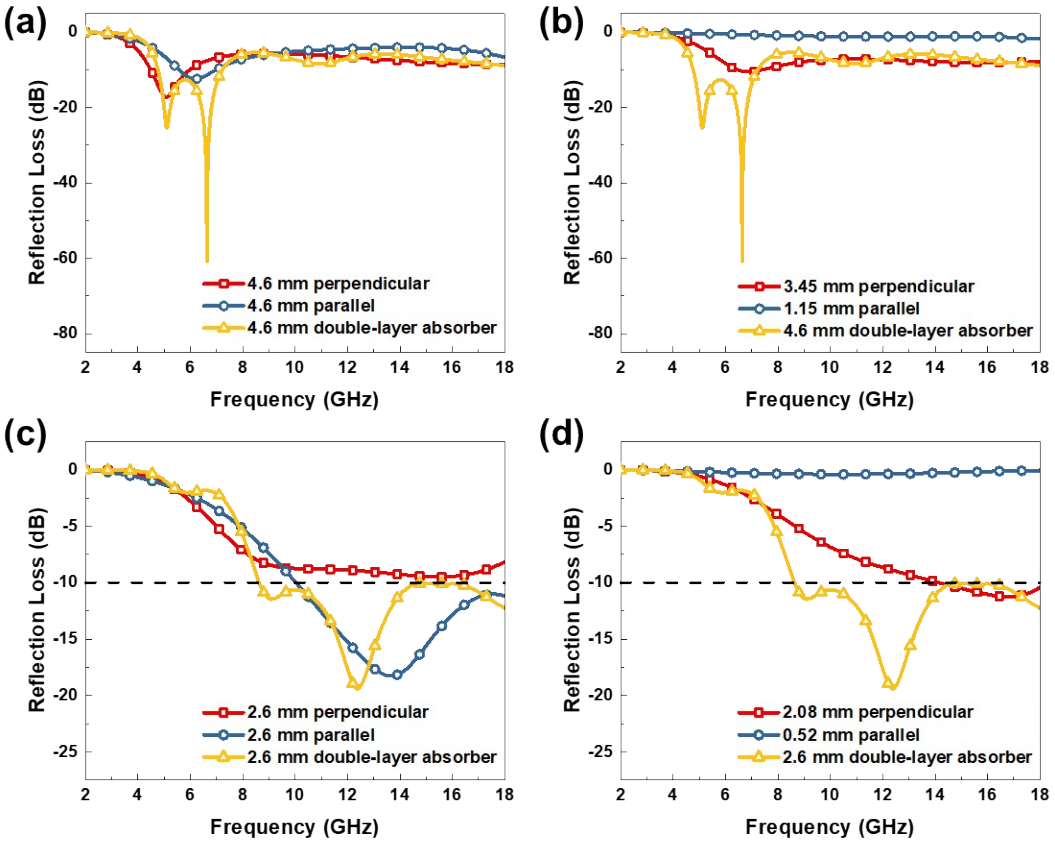


**Fig. S10** (a, c) Comparison of RL curves for single and double layer samples with the same thickness; (b, d) Comparison of RL curves for double-layer samples and their compositions, where parallel end thickness of 25% in (a, b) and 20% in (c, d).

**Table S2** Electromagnetic wave reflection loss for samples with electromagnetic waves incident from the perpendicular ends.

| Matching layer thickness ratio | $RL_{min}$ (dB) | Related Frequency of $RL_{min}$ (GHz) | Related Thickness of $RL_{min}$ (mm) | $EAB_{max}$ (GHz) | Related Thickness of $EAB_{max}$ (mm) |
|---|---|---|---|---|---|
| 5% | -45.2 | 7.3 | 3.8 | 3.4 | 2.3 |
| 10% | -52.7 | 14.8 | 2.2 | 6.4 | 2.5 |
| 15% | -53.0 | 12.1 | 2.5 | 8.4 | 2.6 |
| 20% | -49.0 | 5.5 | 4.6 | 8.1 | 2.5 |
| 25% | -40.6 | 6.5 | 4.5 | 8.4 | 2.5 |
| 30% | -47.6 | 6.7 | 4.4 | 8.6 | 2.5 |
| 35% | -41.3 | 6.8 | 4.3 | 8.8 | 2.5 |
| 40% | -44.1 | 5.0 | 4.4 | 6.3 | 2.4 |
| 45% | -42.6 | 7.0 | 4.2 | 6.0 | 2.4 |
| 50% | -49.0 | 7.0 | 4.0 | 5.5 | 2.4 |
| 55% | -44.9 | 8.0 | 3.2 | 5.1 | 2.3 |
| 60% | -52.0 | 8.0 | 3.2 | 4.8 | 2.2 |
| 65% | -46.7 | 8.0 | 3.2 | 4.1 | 2.3 |
| 70% | -46.8 | 7.2 | 3.9 | 3.8 | 2.3 |
| 75% | -44.4 | 7.8 | 3.3 | 3.7 | 2.3 |
| 80% | -47.1 | 7.8 | 3.3 | 3.6 | 2.3 |
| 85% | -45.8 | 7.8 | 3.3 | 3.5 | 2.3 |
| 90% | -45.0 | 7.3 | 3.8 | 3.5 | 2.3 |
| 95% | -45.2 | 7.3 | 3.8 | 3.4 | 2.3 |

**Table S3** Electromagnetic wave absorption properties of some earlier $Ti_3C_2T_x$ MXene materials

| Samples | $RL_{min}$ (dB) | $EAB_{max}$ (GHz) | Refences |
|---|---|---|---|
| $Ti_3C_2T_x$ MXenes without delamination | ~-7 | 0 | 11 |
| DMF delaminated $Ti_3C_2T_x$ MXenes | -41.9 | ~2.8 | 12 |
| Ethyl alcohol delaminated $Ti_3C_2T_x$ MXene | -17.0 | 5.6 | 13 |
| $Ti_3C_2T_x$ MXenes with Modified Surface | -48.4 | 2.8 | 14 |
| Urchin-like ZnO-$Ti_3C_2T_x$ MXene | -26.3 | 1.4 | 15 |
| 3D PMMA@MXene@$Ni^{2+}$ | -59.6 | 4.5 | 16 |
| Sea urchin-like $Ti_3C_2T_x$ MXene@ZnO hollow spheres | -57.4 | 6.6 | 17 |
| $Ti_3C_2T_x$ MXene@rGO aerogel | -31.2 | 5.4 | 18 |
| $Ti_3C_2T_x$ MXene cellulose aerogel | -43.4 | 4.5 | 19 |
| $Ti_3C_2T_x$ MXene/SiCnws lamellar foam | -55.7 | 4.5 | 20 |
| $Ti_3C_2T_x$ MXene/PI aerogel | -41.8 | 6.5 | 21 |
| Ni/$Ti_3C_2T_x$ MXene/rGO aerogel | -75.2 | 7.3 | 22 |
| $Ti_3C_2T_x$ MXene double-layer absorber with matching layer thickness of 20% | -50.6 | 9.4 | This work |
| $Ti_3C_2T_x$ MXene double-layer absorber with matching layer thickness of 25% | -60.8 | 9.1 | This work |

## References


1. Y. Zhang, Y. Huang, T. Zhang, H. Chang, P. Xiao, H. Chen, Z. Huang and Y. Chen, Advanced Materials, 2015, 27, 2049-2053.

2. X. Li, X. Yin, H. Xu, M. Han, M. Li, S. Liang, L. Cheng and L. Zhang, Acs Applied Materials & Interfaces, 2018, 10, 34524-34533.

3. M. Naguib, M. Kurtoglu, V. Presser, J. Lu, J. Niu, M. Heon, L. Hultman, Y. Gogotsi and M. W. Barsoum, Advanced Materials, 2011, 23, 4248-4253.

4. J. Zhang, N. Kong, S. Uzun, A. Levitt, S. Seyedin, P. A. Lynch, S. Qin, M. Han, W. Yang, J. Liu, X. Wang, Y. Gogotsi and J. M. Razal, Advanced Materials, 2020, 32.

5. S. Zhao, H.-B. Zhang, J.-Q. Luo, Q.-W. Wang, B. Xu, S. Hong and Z.-Z. Yu, Acs Nano, 2018, 12, 11193-11202.

6. Z. Wu, T. Shang, Y. Deng, Y. Tao and Q.-H. Yang, Advanced Science, 2020, 7.

7. B. Anasori, M. R. Lukatskaya and Y. Gogotsi, Nature Reviews Materials, 2017, 2.

8. M. Ghidiu, M. R. Lukatskaya, M.-Q. Zhao, Y. Gogotsi and M. W. Barsoum, Nature, 2014, 516, 78-U171.

9. G. Wang, X. Peng, L. Yu, G. Wan, S. Lin and Y. Qin, Journal of Materials Chemistry A, 2015, 3, 2734-2740.

10. Z. Cheng, Y. Cao, R. Wang, L. Xia, S. Ma, Z. Li, Z. Cai, Z. Zhang and Y. Huang, Carbon, 2021, 185, 669-680.

11. M. Han, X. Yin, X. Li, B. Anasori, L. Zhang, L. Cheng and Y. Gogotsi, Acs Applied Materials & Interfaces, 2017, 9, 20038-20045.

12. G. Xu, X. Wang, S. Gong, S. Wei, J. Liu and Y. Xu, Nanotechnology, 2018, 29.

13. Y. Qing, W. Zhou, F. Luo and D. Zhu, Ceramics International, 2016, 42, 16412-16416.

14. M. Han, X. Yin, H. Wu, Z. Hou, C. Song, X. Li, L. Zhang and L. Cheng, Acs Applied Materials & Interfaces, 2016, 8, 21011-21019.

15. Y. Qian, H. Wei, J. Dong, Y. Du, X. Fang, W. Zheng, Y. Sun and Z. Jiang, Ceramics International, 2017, 43, 10757-10762.

16. C. Wen, X. Li, R. Zhang, C. Xu, W. You, Z. Liu, B. Zhao and R. Che, Acs Nano, 2022, 16, 1150-1159.

17. Y.-Q. Wang, H.-B. Zhao, J.-B. Cheng, B.-W. Liu, Q. Fu and Y.-Z. Wang, Nano-Micro Letters, 2022, 14.

18. L. Wang, H. Liu, X. Lv, G. Cui and G. Gu, Journal of Alloys and Compounds, 2020, 828.

19. Y. Jiang, X. Xie, Y. Chen, Y. Liu, R. Yang and G. Sui, Journal of Materials Chemistry C, 2018, 6, 8679-8687.

20. X. Li, X. Yin, H. Xu, M. Han, M. Li, S. Liang, L. Cheng and L. Zhang, Acs Applied Materials & Interfaces, 2018, 10, 34524-34533.

21. Y. Dai, X. Wu, Z. Liu, H.-B. Zhang and Z.-Z. Yu, Composites Part B-Engineering, 2020, 200.

22. L. Liang, Q. Li, X. Yan, Y. Feng, Y. Wang, H.-B. Zhang, X. Zhou, C. Liu, C. Shen and X. Xie, Acs Nano, 2021, 15, 6622-6632.